Fabrication of Anodic Porous Alumina via Galvanostatic Anodizing in Alkaline Sodium Tetraborate Solution and Their Morphology

Tatsuya Kikuchi[*,a], Kaito Kunimoto[a], Hiroki Ikeda[a], Daiki Nakajima[a], Ryosuke O. Suzuki[a], Shungo Natsui[b]
[a]Faculty of Engineering, Hokkaido University, N13-W8, Kita-ku, Sapporo, Hokkaido, 060-8628, Japan
[b]Institute of Multidisciplinary Research for Advanced Materials, Tohoku University, Katahira 2-1-1, Aoba-ku, Sendai, Miyagi, 980-8577, Japan

*Corresponding author: Tatsuya Kikuchi
TEL: +81-11-706-6340
FAX: +81-11-706-6342
E-mail: kiku@eng.hokudai.ac.jp

Abstract

The anodizing of aluminum in an alkaline sodium tetraborate ($Na_2B_4O_7$) solution was investigated with respect to the nanostructural characterization of anodic porous alumina. Electropolished aluminum specimens were galvanostatically anodized under various conditions in 0.1-0.5 M sodium tetraborate solutions at 293-353 K and a current density of 2.5-400 Am^{-2}. Anodic oxide with numerous flower-like defects was formed by anodizing in a 0.1 M $Na_2B_4O_7$ solution due to the film breakdown with continuous visible sparking. On the other hand, a uniform porous alumina film without any breakdown was successfully obtained by anodizing a more concentrated solution than 0.3 M at 333 K. The anodic oxide was almost pure alumina and consisted of a thin outer layer with numerous small pits and a thick inner layer with typical porous alumina cells. The pore walls possessed continuous bumpy surfaces measuring 10-20 nm in roughness. As the temperature further increased to 353 K, the regularity of the porous alumina improved due to the high current density of more than 150 Am^{-2} during anodizing. Slippery superhydrophobic and sticky superoleophobic aluminum surfaces could be easily fabricated via high temperature anodizing and subsequent self-assembled monolayer modification.

Keywords: Aluminum, Anodizing, Porous Alumina, Sodium Tetraborate, Nanostructure

1. Introduction

A porous type anodic oxide film (anodic porous alumina) of Al possesses a unique hexagonal honeycomb structure with numerous nanoscale pores, and it can be typically obtained by anodizing (anodization) aluminum in several acidic solutions such as phosphoric (H_3PO_4) [1], chromic (H_2CrO_4) [2], oxalic ($(COOH)_2$) [3], and sulfuric (H_2SO_4) acids [4,5]. The porous alumina film has been widely used in various industries for the corrosion protection [6,7], coloring [8], and hardening [9,10] of Al alloys since the beginning of the 20th century. Notably, the self-ordering behavior of the honeycomb structure during anodizing under appropriate operating conditions was found by Masuda et al. at the end of the 1990s [11-13]. The discovery expanded the applicability of the porous alumina in various nanoscience and nanoengineering fields [14-18]. Because the nanostructure and chemical, physical, and optical properties of the porous alumina strongly depend on the electrolyte species used [19-21], additional acidic electrolytes have been investigated by many research groups with respect to the formation of novel porous alumina. Inorganic acids [22-28], organic carboxylic acids [29-35], organophosphorus acids [36-41], and cyclic oxocarbon acids [42,43] have been studied so far.

Although it is known that the porous alumina film can also be formed by anodizing aluminum in alkaline solutions, extremely little has been reported on the anodizing behavior and its nanostructural characterization. In 1969, Leach et al. reported the structure and properties of anodic films grown in an ammonium hydrogen tetraborate solution with ammonium hydroxide [44]. The oxide films show typical barrier or porous growth based on the temperature of the solution. In 1973, John et al. investigated the effects of the electrochemical conditions on the formation rate of anodic oxide formed by anodizing aluminum in sodium tetraborate solution ($Na_2B_4O_7$, borax) [45]. The thickness of the anodic oxide increased with the pH and the temperature except for those films that were grown at the highest temperatures and pH values. However, no clear micro- or nanoscopic image of the anodic oxide was provided in these investigations. In later years, Thompson et al. reported on the initial growth behavior of the porous alumina formed by anodizing at a constant voltage of 60 V in a $Na_2B_4O_7$ solution [46,47]. They found that the porous alumina film possessed the characteristic feathered pore morphology. However, the anodizing was limited by narrow conditions of 60 V and 333 K in this investigation. Therefore, the details of the anodizing behavior in various electrochemical conditions and the subsequent nanostructure obtained in alkaline solutions are still unknown.

In the present investigation, we described the details of the electrochemical behaviors and nanostructural characterization of the porous alumina that is formed by galvanostatic anodizing in an alkaline $Na_2B_4O_7$ solution. The effects of the concentration, temperature, and current density on the anodizing behavior were investigated with respect to the fabrication of porous alumina. In addition, the nanostructure of the porous alumina was examined using electron microscopy and chemical composition analysis. Furthermore, slippery superhydrophobic and sticky superoleophobic Al surfaces were fabricated using alkaline anodizing at high temperature and a subsequent water repellent process.

2. Experimental

2.1 Pretreatments

Al plates (99.999 wt%, 250 μm thick, GoodFellow, UK) were cut into pieces 20 mm in length and 10 mm in width with an electroconductive handle and were ultrasonically degreased in 99.5 % ethanol (C_2H_5OH) for 10 min. After ultrasonication, the bottom of the handle was covered with a silicone resin in order to fix the anodizing area of the Al specimens. The resin-coated Al specimens were immersed in a 78 vol% acetic acid (CH_3COOH)/22 vol% perchloric acid ($HClO_4$, assay: 70 %) solution at 280 K and were electrochemically polished at a constant voltage of 28 V for 1 min.

2.2 Anodizing

The electropolished Al specimen as the anode and a Pt plate (99.95 wt%, 100 μm thick, Furuya Metal, Japan) as the cathode were immersed in an electrochemical cell with 0.05-0.5 M of $Na_2B_4O_7$ solutions (150 mL) at 293-353 K. The Al specimens were anodized at a constant current density of 2.5-400 Am^{-2} for up to 7 h using a direct power supply (PWR400H, Kikusui, Japan). The electrolyte solution was stirred at 250 rpm with a magnetic stirrer during anodizing, and the temperature was adjusted to each operating value using a constant-temperature bath (UCT-1000 for 293-333 K and OBS-200AM for 353 K, As one, Japan). The pH of the electrolyte solutions was measured with a benchtop pH meter (SevenMulti, Mettler Toledo, USA).

2.3 SEM observations

The surface and fracture cross-section of the anodized specimens were examined using field-emission scanning electron microscopy (FE-SEM, JSM-6500F, JEOL, Japan). Before the SEM observations, a thin electroconductive Pt layer was formed on the anodic oxide using a sputter coater (MSP-1S, Vacuum Device, Japan). The anodized specimens were immersed in a 0.20 M CrO_3/0.51 M H_3PO_4 solution at 353 K to dissolve the anodic oxide, and the exposed Al surfaces were also examined by SEM.

2.4 STEM observations

Ultrathin horizontal cross-sections prepared by precision polishing with an Ar ion beam and the vertical cross-sections formed by ultrathin sectioning with an ultramicrotome were examined using Cs-corrected scanning transmission electron microscopy (STEM, Titan3 G2 60-300, FEI). The details of the preparation of these specimens have been given elsewhere [48]. The qualitative analysis of the porous alumina films was conducted using energy dispersive X-ray spectrometry (EDS) and electron energy-loss spectroscopy (EELS).

2.5 Contact angle measurements

The anodized specimens were immersed in a 0.5 mM 3,3,4,4,5,5,6,6,7,7,8,8,8-tridecafluorooctylphosphonic acid ($C_8H_6F_{13}O_3P$, FOPA)/C_2H_5OH solution at 313 K for 24 h, and the surface of the anodic oxide was modified using a FOPA self-assembled monolayer (SAM). Commercially available rapeseed oil and ultrapure water (18.2 MΩ·cm) drops were formed on the specimens using a microsyringe connected to an auto dispenser with a flow rate of 2 μLs^{-1}, and the advancing contact angle (θ_{adv}) and receding contact angle (θ_{rec}) were measured using an optical contact angle meter (DM-501, Kyowa Interface Science, Japan). A circle fitting of the drops was performed for the measurements of the θ_{adv} and θ_{rec} values.

3. Results and Discussion

The electropolished Al specimens were anodized in an alkaline $Na_2B_4O_7$ solution under various conditions. Figure 1a shows the changes in the voltage, U_a, with time, t_a, during anodizing in a 0.1 M $Na_2B_4O_7$ solution at 293 K (pH = 9.3) and a constant current density of 2.5-20 Am^{-2}. The voltage linearly increased with the anodizing time at a low current density of 2.5 Am^{-2}, and exhibited a steady value measuring approximately 400 V after long-term anodizing for 110 min. Continuous visible sparking was observed on the Al surface at this steady voltage. The linear slope of the voltage-time curves during the initial stage increased with the current density, and visible sparking also occurred at each current density as the voltage reached approximately 400 V. Similar anodizing behaviors with linear increases in the initial stage and visible sparking at high voltages were obtained by anodizing aluminum in a 0.1 M

$Na_2B_4O_7$ solution at a higher temperature of 313 K (Fig. 1b, pH = 9.1).

As the temperature of the $Na_2B_4O_7$ solution further increased to 333 K (Fig. 1c, pH = 9.0), the characteristic voltage-time curves for the formation of porous alumina were measured at a medium current density range of 75-125 Am^{-2}. Here, the voltage linearly increased during the initial stage of anodizing, reached a maximum value, and then gradually decreased with the anodizing time. In the typical case of anodizing in phosphoric, oxalic, and sulfuric acid solutions for the porous alumina, the voltage remains at an almost steady value after this gradual decrease [19,20,49]. However, the voltage increased once again via long-term anodizing in the $Na_2B_4O_7$ solution, and visible sparking occurred on the Al surface at more than 450 V. No voltage increase was measured at a low current density of 25 Am^{-2}, and a linear increase and subsequent visible sparking occurred at a high current density of 150 Am^{-2}.

Figure 2a shows an SEM image of the typical surface of the specimen that is anodized at 293 K and 2.5 Am^{-2} (Fig. 1a) with a linear increase and visible sparking. The Al surface was covered with numerous flower-like defects originating from the breakdown and continuous sparking, and there is no uniform porous alumina on the surface under these conditions. These nanostructures are similar to the formation of the barrier oxide film and the subsequent breakdown during anodizing in neutral electrolyte solutions [50]. In contrast, Figure 2b shows an SEM image of the surface of the specimen that is anodized at a higher temperature of 333 K and 75 Am^{-2} (Fig. 1c). Because the typical voltage-time curve for the porous alumina was measured under these conditions, numerous nanoscale pores measuring approximately 200 nm in diameter were distributed on the entire surface, and porous alumina was successfully obtained by anodizing at high temperature. However, continuous sparking caused by the breakdown was observed via the excess anodizing at more than 450 V. This is due to the low solubility of the anodic oxide in the low concentration solution. The thickness of the barrier layer may increase with the anodizing time, thus long-term anodizing causes the film breakdown with continuous visible sparking. Therefore, the stable anodizing conditions without any film breakdown were further investigated.

Figure 3 illustrates the effect of the concentration of the $Na_2B_4O_7$ solution on the anodizing behaviors. Because the saturated solubility of $Na_2B_4O_7 \cdot 10H_2O$ in water has a low value of 0.134 M at 293 K, the temperature of the solution was adjusted to a high temperature of 333 K for the overall anodizing conditions. At the low concentration of 0.05 M (Fig. 3a, pH = 8.9), the voltage was gradually increased over time during anodizing, and continuous sparking was observed on the Al specimen. Therefore, the use of a low concentration $Na_2B_4O_7$ solution is inappropriate for the formation of porous alumina. In contrast, stable voltage-time curves without excess voltage increases were successfully obtained during anodizing at relatively high concentrations of 0.3 M (Fig. 3b, pH = 9.0) and 0.5 M (Fig. 3c, pH = 9.1) under appropriate current densities, and no visible sparking was observed on the Al surface during anodizing. The plateau voltage increased with the current density in either concentration, and the excess current densities such as 75 Am^{-2} in the 0.3 M solution and 40 Am^{-2} in the 0.5 M solution caused the immediate breakdown of the film with continuous sparking. The maximum current density without any film breakdown decreased as the concentration increased.

Figure 4 shows the SEM images of the surface and fracture cross-section of the specimen that was anodized in a 0.3 M $Na_2B_4O_7$ solution at 333 K for 120 min under various current density conditions, which is shown in Fig. 3b. Nonuniform anodic oxide with fibrous nanostructures formed on the Al surface at a lower current density of 15 Am^{-2} (Fig. 4a) because the extremely low voltage measuring less than 5 V was maintained during anodizing. This nanomorphology is very similar to the surface of the porous alumina that was chemically dissolved into the electrolyte solution via long-term anodizing at high temperature. As the current density increased to 30 Am^{-2} and 50 Am^{-2} (Fig. 4b and 4c), clear porous alumina films with vertical nanoscale pores were formed on the Al surface. Characteristically, the porous alumina possessed a two-layer nanostructure consisting of a thin outer layer with numerous small pits and

a thick inner layer with typical porous alumina cells. The cell size of the inner porous alumina layer increased with the current density due to the increasing anodizing voltage. To measure the cell size, the porous alumina film was dissolved in a CrO_3/H_3PO_4 solution.

Figures 5a and 5b show the SEM images of the exposed Al surface after anodizing in a 0.3 M $Na_2B_4O_7$ solution at 333 K and a) 25 Am^{-2} and b) 50 Am^{-2}, respectively, for 120 min. Numerous small dimples measuring approximately 180 nm in cell size were distributed on the Al surface that formed at 25 Am^{-2} (Fig. 5a) due to the relatively low voltage of 58 V after 120 min of anodizing. As the current density increased to 50 Am^{-2} (Fig. 5b), the voltage increased to 230 V and the average cell size also increased to 630 nm. Because the anodizing in the 0.3 M and 0.5 M $Na_2B_4O_7$ solutions at 333 K under appropriate current densities successfully leads to the formation of porous alumina, the change in the cell size that was calculated using the SEM images, D_c, with the anodizing voltage after 120 min of anodizing, U_a, is shown in Figure 5c. Here, a yellow line corresponds to the linear relationship between the cell size and the anodizing voltage that is obtained by the typical anodizing in acidic solutions [19,20]:

$$D_c = 2.5\ U_a \qquad (1)$$

The cell size linearly increased with the anodizing voltage at each current density, and this result is in good agreement with the linear relation of equation (1). Therefore, the average cell size of the porous alumina that formed in the alkaline $Na_2B_4O_7$ solution can be controlled by the choosing the appropriate current density and the corresponding anodizing voltage.

From the above experimental results, the anodizing in a high concentration $Na_2B_4O_7$ solution at high temperature causes the formation of thick porous alumina without any film breakdown. The nanostructural characterization of the porous alumina was further investigated in detail using SEM and TEM observations. Figure 6 shows the high-magnification SEM images of the porous alumina that was formed by anodizing in a) 0.3 M and b) 0.5 M $Na_2B_4O_7$ solutions, respectively, at 333 K and 30 Am^{-2}. Because the anodizing was conducted using the galvanostatic method, disordered porous alumina with nonstraight nanopores were observed on the cross-sectional SEM images. Notably, the pore walls possessed uneven nanomorphologies without smooth planes. This morphology is different from the pore walls of the porous alumina that is formed by typical anodizing in phosphoric, oxalic, and sulfuric acids but is similar to that formed by chromic acid anodizing [51,52].

The porous alumina film shown in Fig. 6b was horizontally thinned using Ar ion irradiation for the STEM observations. Figure 7a shows a HAADF-STEM image of the horizontally thinned specimen. Disordered nanoscale pores with different diameters measuring several hundreds of nanometers were distributed in the porous alumina due to galvanostatic anodizing without self-ordering. In addition, there was no clear honeycomb distribution with a cell boundary (skeleton) in the porous alumina. A high-magnification HAADF-STEM image of the typical nanopore is shown in Figure 7b. The pore wall possessed a continuous bumpy surface measuring 10-20 nm in roughness, which is same as the fracture cross-sections.

Figures 7c-7e provide the bright-field (BF) TEM images of the vertical cross-section of the porous alumina. Here, the porous alumina film was thinned to 20 nm thick using diamond knife and an ultramicrotome, and the bottom Al substrate was removed from the porous alumina during the ultramicrotomy. The outermost layer of the porous alumina consisted of many small pits measuring approximately 10-20 nm in diameter, and the thickness of this outer layer is very thin at approximately 100 nm (Fig. 7d). Larger pores measuring several hundreds of nanometers in diameter grew in the inner layer (Fig. 7c), and these pore walls possessed a top-to-bottom feathered morphology.

The incorporated anion distribution in the porous alumina was examined using EDS and EELS. Figure 8a shows the BF-TEM image and the corresponding elemental distribution maps of the Al, O, and B of the vertical cross-section of the porous alumina. The Al and O distributions corresponding to the

configuration of the porous alumina were clearly measured from the EDS mapping images. In contrast, there was almost no B originating from the electrolyte anion ($B_4O_7^{2-}$). Figure 8b illustrates the EDS spectrum of the whole vertical cross-section that is shown in Fig. 8a. Although three clear peaks for Al and O originating from the porous alumina and the carbon from the contamination and two small peaks for Cu and Si originating from the TEM grid were measured from the specimen, there was no peak for B. Figures 8c and 8d show the HAADF-STEM image and corresponding EELS spectra of the horizontal cross-section of the porous alumina. Although similar EELS results with a clear C-K peak and a small Ar-$L_{2,3}$ edge peak originating from Ar ion irradiation were obtained at two different positions, as shown in Fig. 8c, there was no B-K peak on the EELS spectra. From the above EDS and EELS analysis, the porous alumina that was formed using anodizing in a $Na_2B_4O_7$ solution consisted of almost pure alumina.

The nanostructure and composition of this porous alumina is extremely similar to that formed by anodizing in chromic acid. The nanostructural features of the porous alumina that was formed in chromic acid have been reported as follows [51,52]. a) Extremely disordered porous alumina possessing feathered pore walls is formed using anodizing under constant current and voltage processes. b) A characteristic branched colony pore structure is observed in the inner layer of the porous alumina. c) The porous alumina consists of pure Al_2O_3 without an electrolyte anion and, thus, a honeycomb skeleton is not evident in the porous alumina. Because these characteristics are the same as those of the porous alumina that formed in $Na_2B_4O_7$, this porous alumina may grow under a similar growth mechanism.

Hebert et al. reported that the typical porous alumina that was obtained by phosphoric, oxalic, and sulfuric acids is mainly formed through the field-assisted flow mechanism [53,54]. The flow of the oxide is produced by the rapid formation of O^{2-} at the bottom of the pores during anodizing. Ordered porous alumina is empirically obtained by anodizing in these electrolyte solutions through the field-assisted flow mechanism. Conversely, Thompson et al. reported that the porous alumina that was formed by chromic acid and $Na_2B_4O_7$ is mainly formed through the field-assisted dissolution mechanism without the oxide flow [55,56]. In these cases, disordered porous alumina with a pore-branching structure is empirically obtained using anodizing. However, we found that galvanostatic anodizing at further higher temperatures improved the regularity of the porous alumina.

Figure 9 shows the changes in the voltage, U_a, with time, t_a, during anodizing in a 0.5 M $Na_2B_4O_7$ solution at 353 K (pH = 8.9) and a constant current density of i = 50-400 Am^{-2}. As the temperature increased to 353 K from 333 K (Fig. 3c), larger current densities without visible sparking could be applied to the Al specimen. The anodizing voltage increased with the current density, and unstable oscillations were measured during anodizing at a current density of more than 200 Am^{-2}. Although the voltage gradually increased with the anodizing time at these high current densities, no visible spark was observed on these Al specimens.

Figure 10 provides the SEM images of the surface (left), fracture cross-section (center), and corresponding Al dimple array (right) of the porous alumina formed at a) 150 Am^{-2} and b) 200 Am^{-2}, respectively. Bundled structures consisting of several tens or hundreds of alumina nanofibers were formed on each surface (left in Fig. 10). These characteristic nanostructures were due to the chemical dissolution of the outermost layer of the porous alumina during anodizing in a concentrated $Na_2B_4O_7$ solution at high temperature. Interestingly, the fracture cross-section images of the porous alumina that was formed under the pyramidal bundles exhibited high regularity with numerous straight nanopores (center in Fig. 10). An ordered cell arrangement consisting of several tens of dimples can be observed on the Al surface that was formed by the dissolution of porous alumina (right in Fig. 10). This self-ordering behavior may be due to the high current density during anodizing without any film breakdown at a high concentration and high temperature. However, the galvanostatic method is inappropriate for the formation of highly ordered porous alumina due to the changes of the applied voltage during anodizing. Usually, ordered porous

alumina can be fabricated by anodizing at appropriate constant voltages under high current density conditions [26]. Therefore, further investigations of the constant voltage of anodizing in a $Na_2B_4O_7$ solution at high temperature are required to find the new self-ordering regime.

We found that alumina nanofiber structures that are modified with low surface energy molecules exhibited slippery superhydrophobic and sticky superoleophobic behaviors. The pyramidal alumina bundled structures that were fabricated through anodizing were modified with FOPA-SAM. Figure 11a shows the appearance of ultrapure water droplets during the advancing and receding contact angle measurements. The θ_{adv} and θ_{rec} values of the water droplets that were measured on the pyramidal structures were 165.5° and 162.6°, respectively. Because the contact angle hysteresis (θ_{adv} - θ_{rec}) is calculated as 2.9°, highly slippery superhydrophobic Al was successfully fabricated via our anodizing and SAM modification processes. Conversely, the sticky superoleophobic property with high contact angle hysteresis appeared using a rapeseed oil with low surface tension (θ_{adv} = 157.5° and θ_{rec} = 0°, Fig. 11b). Surface wettability strongly depends on the surface tension of the droplet and the nanomorphology of the anodic oxide formed by anodizing [57,58]. Therefore, more complicated nanostructures such as a multiscale hierarchical structure are required for the slippery superoleophobic surface.

4. Conclusions

Electropolished Al specimens were anodized under various conditions in 0.05-0.5 M sodium tetraborate solutions at 293-353 K and constant current densities of 2.5-400 Am^{-2}. The anodizing behaviors and corresponding nanostructures were concluded as follows.

1) The galvanostatic anodizing of Al in a low concentration of 0.1 M $Na_2B_4O_7$ solution leads to the formation of anodic oxide with numerous defects due to the continuous visible sparking.

2) As the concentration increases to more than 0.3 M at a high temperature of 333 K, a porous alumina film without any breakdown defect grows on the Al surface.

3) The porous alumina consists of a thin outer layer with numerous small pits and a thick inner layer with typical porous alumina cells. The pore walls possess continuous bumpy surfaces measuring 10-20 nm in roughness. The anodic oxide is almost pure alumina.

4) As the temperature further increases to 353 K, the regularity of the porous alumina improves due to the high current density of more than 150 Am^{-2} during anodizing without any film breakdown.

5) Slippery superhydrophobic and sticky superoleophobic Al surfaces can be easily fabricated via high temperature anodizing and subsequent FOPA-SAM modification.

Acknowledgments

The authors would like to thank Mr. Nobuyuki Miyazaki, Dr. Takashi Endo, and Mr. Ryo Oota for their help with the electron microscopy. This study was supported in part by the Salt Science Research Foundation, the Fundamental Research Developing Association for Shipbuilding and Offshore, and the Nanotechnology Platform Program of the MEXT-Japan.

References

1) H. Masuda, K. Yada, A. Osaka, Self-ordering of cell configuration of anodic porous alumina with large-size pores in phosphoric acid solution, Jpn. J. Appl. Phys. 37 (1998) L1340.

2) W.J. Stępniowski, M. Michalska-Domańska, M. Norek, T. Czujko, Fast Fourier transform based arrangement analysis of poorly organized alumina nanopores formed via self-organized anodization in chromic acid, Mater. Lett. 117 (2014) 69-73.

3) G.D. Sulka, W.J. Stępniowski, Structural features of self-organized nanopore arrays formed by anodization of aluminum in oxalic acid at relatively high temperatures, Electrochim. Acta 54 (2009)

3683-3691.
4) G.D. Sulka, S. Stroobants, V. Moshchalkov, G. Borghs, J.P. Celis, Synthesis of well-ordered nanopores by anodizing aluminum foils in sulfuric acid, J. Electrochem. Soc. 149 (2002) D97-D103.
5) H. Asoh, K. Nishio, M. Nakao, A. Yokoo, T. Tamamura, H. Masuda, Fabrication of ideally ordered anodic porous alumina with 63 nm hole periodicity using sulfuric acid, J. Vac. Sci. Technol. B 19 (2001) 569-572.
6) X. Li, X. Nie, L. Wang, D.O. Northwood, Corrosion protection properties of anodic oxide coatings on an Al–Si alloy, Surf. Coat. Technol. 200 (2005) 1994-2000.
7) T. Kikuchi, Y. Hara, M. Sakairi, T. Yonezawa, A. Yamauchi, H. Takahashi, Corrosion of Al–Sn–Bi alloys in alcohols at high temperatures. Part II: Effect of anodizing on corrosion, Corr. Sci. 52 (2010) 2525-2534.
8) C.J. Donahue, J.A. Exline, Anodizing and coloring aluminum alloys, J. Chem. Educ. 91 (2014) 711-715.
9) L.E. Fratila-Apachitei, J. Duszczyk, L. Katgerman, Vickers microhardness of AlSi(Cu) anodic oxide layers formed in H_2SO_4 at low temperature, Surf. Coat. Technol. 165 (2003) 309-315.
10) T. Kikuchi, A. Takenaga, S. Natsui, R.O. Suzuki, Advanced hard anodic alumina coatings via etidronic acid anodizing, Surf. Coat. Technol. 326 (2017) 72-78.
11) H. Masuda, K. Fukuda, Ordered metal nanohole arrays made by a two-step replication of honeycomb structures of anodic alumina, Science 268 (1995) 1466-1468.
12) H. Masuda, H. Yamada, M. Satoh, H. Asoh, M. Nakao, T. Tamamura, Highly ordered nanochannel-array architecture in anodic alumina, Appl. Phys. Lett. 71 (1997) 2770-2772.
13) H. Masuda, F. Hasegwa, S. Ono, Self−ordering of cell arrangement of anodic porous alumina formed in sulfuric acid solution, J. Electrochem. Soc. 144 (1997) L127-L130.
14) T. Kondo, H. Miyazaki, T. Yanagishita, H. Masuda, Anodic porous alumina with elliptical apertures, Electrochem. Commun. 96 (2018) 61-65.
15) T. Yanagishita, M. Imaizumi, T. Kondo, H. Masuda, Preparation of nanoporous alumina hollow spheres with a highly ordered hole arrangement, RSC Adv. 8 (2018) 2041-2047.
16) L. Wen, R. Xu, Y. Mi, Y. Lei, Multiple nanostructures based on anodized aluminium oxide templates, Nat. Nanotechnol. 12 (2017) 244-250.
17) T. Ozel, G.R. Bourret, C.A. Mirkin, Coaxial lithography, Nat. Nanotechnol. 10 (2015) 319-324.
18) C.Y. Peng, C.W. Hsu, C.W. Li, P.L. Wang, C.C. Jeng, C.C. Chang, G.J. Wang, Flexible photonic crystal material for multiple anticounterfeiting applications, ACS Appl. Mater. Interfaces 10 (2018) 9858-9864.
19) W. Lee, D. J. Park, Porous anodic aluminum oxide: anodization and templated synthesis of functional nanostructures, Chem. Rev., 114 (2014) 7487-7556.
20) G.D. Sulka, Highly ordered anodic porous alumina formation by self-organized anodizing, in: A. Eftrkhari (Ed.), Nanostructured materials in electrochemistry, Wiley-VCH Verlag GmbH & Co. KGaA, Weinheim, 2008, pp. 1-116.
21) T. Kikuchi, D. Nakajima, O. Nishinaga, S. Natsui, R.O. Suzuki, Porous aluminum oxide formed by anodizing in various electrolyte species, Curr. Nanosci. 11 (2015) 560-571.
22) T. Kikuchi, O. Nishinaga, S. Natsui, R.O. Suzuki, Self-ordering behavior of anodic porous alumina via selenic acid anodizing, Electrochim. Acta 137 (2014) 728-735.
23) S. Akiya, T. Kikuchi, S. Natsui, R.O. Suzuki, Optimum exploration for the self-ordering of anodic porous alumina formed via selenic acid anodizing, J. Electrochem. Soc. (2015) E244-E250.
24) Y. Nazarkina, S. Gavrilov, H. Terryn, M. Petrova, J. Ustarroz, Investigation of the ordering of porous anodic alumina formed by anodization of aluminum in selenic acid, J. Electrochem. Soc.

(2015) E166-E172.
25) A.I. Sadykov, S.E. Kushnir, I.V. Roslyakov, A.E. Baranchikov, K.S. Napolskii, Selenic acid anodizing of aluminium for preparation of 1D photonic crystals, Electrochem. Commun. 100 (2019) 104-107.
26) S. Akiya, T. Kikuchi, S. Natsui, N. Sakaguchi, R.O. Suzuki, Self-ordered porous alumina fabricated via phosphonic acid anodizing, Electrochim. Acta 190 (2016) 471-479.
27) S. Stojadinovic, Z. Nedic, I. Belca, R. Vasilic, B. Kasalica, M. Petkovic, L. Zekovic, The effect of annealing on the photoluminescent and optical properties of porous anodic alumina films formed in sulfamic acid, Appl. Surf. Sci. 256 (2009) 763-767.
28) S. Akiya, T. Kikuchi, S. Natsui, R.O Suzuki, Nanostructural characterization of large-scale porous alumina fabricated via anodizing in arsenic acid solution, Appl. Surf. Sci. 403 (2017) 652-661.
29) M. Norek, M. Włodarski, Morphological and chemical characterization of highly ordered conical-pore anodic alumina prepared by multistep citric acid anodizing and chemical etching process, Porous Mater. 25 (2018) 45-53.
30) Y. Ma, Y. Wen, J. Li, Y. Li, Z. Zhang, C. Feng, R. Sun, Fabrication of self-ordered alumina films with large interpore distance by Janus anodization in citric acid, Sci. Rep. 6 (2016) 39165.
31) G. Knörnschild, A.A. Poznyak, A.G. Karoza, A. Mozalev, Effect of the anodization conditions on the growth and volume expansion of porous alumina films in malonic acid electrolyte, Surf. Coat. Technol. 275 (2015) 17-25.
32) M. Pashchanka, J.J. Schneider, Formation of porous anodic alumina under unstable electroconvection flow regimes: A case study of tartronic acid electrolyte, J. Phys. Chem. C 121 (2017) 23683-23692.
33) T. Kikuchi, O. Nishinaga, S. Natsui, R.O. Suzuki, Fabrication of anodic nanoporous alumina via acetylenedicarboxylic acid anodizing, ECS Electrochem. Lett. 3 (2014) C25-C28.
34) D. Nakajima, T. Kikuchi, S. Natsui, R.O. Suzuki, Growth behavior of anodic oxide formed by aluminum anodizing in glutaric and its derivative acid electrolytes, Appl. Surf. Sci. 321 (2014) 364-370.
35) I.A. Vrublevsky, K.V. Chernyakova, A. Ispas, A. Bund, S. Zavadski, Optical properties of thin anodic alumina membranes formed in a solution of tartaric acid, Thin Solid Films 556 (2014) 230-235.
36) T. Kikuchi, O. Nishinaga, S. Natsui, R.O. Suzuki, Fabrication of self-ordered porous alumina via etidronic acid anodizing and structural color generation from submicrometer-scale dimple array, Electrochim. Acta 156 (2015) 235-243.
37) A. Takenaga, T. Kikuchi, S. Natsui, R.O. Suzuki, Exploration for the self-ordering of porous alumina fabricated via anodizing in etidronic acid, Electrochim. Acta 211 (2016) 515-523.
38) T. Kikuchi, A. Takenaga, S. Natsui, R.O. Suzuki, Advanced hard anodic alumina coatings via etidronic acid anodizing, Surf. Coat. Technol. 326 (2017) 72-78.
39) M. Sepúlveda, J.G. Castaño, F. Echeverría, Influence of temperature and time on the fabrication of self-ordering porous alumina by anodizing in etidronic acid, Appl. Surf. Sci. 454 (2018) 210-217.
40) H. Huang, J. Qiu, M. Sun, W. Liu, X. Wei, E. Sakai, K. Ito, A hard coating with MAO/AAO double layers prepared on aluminum in etidronic acid by DC oxidation, Surf. Coat. Technol. 360 (2019) 307-317.
41) A. Takenaga, T. Kikuchi, S. Natsui, R.O. Suzuki, Self-ordered aluminum anodizing in phosphonoacetic acid and its structural coloration, ECS Solid State Lett. 4 (2015) P55-P58.
42) T. Kikuchi, T. Yamamoto, S. Natsui, R.O. Suzuki, Fabrication of anodic porous alumina by squaric acid anodizing, Electrochim. Acta 123 (2014) 14-22.
43) T. Kikuchi, D. Nakajima, J. Kawashima, S. Natsui, R.O. Suzuki, Fabrication of anodic porous

alumina via anodizing in cyclic oxocarbon acids, Appl. Surf. Sci. 313 (2014) 276-285.
44) J.L. Leach, P. Neufeld, Pore structure in anodic Al_2O_3 films, Corr. Sci. 9 (1969) 413-421.
45) S. John, V. Balasubramanian, B.A. Shenoi, Studies on anodizing of aluminium in alkaline electrolyte using alternating current, Surf. Technol. 26 (1985) 207-216.
46) A. Pakes, G.E. Thompson, P. Skeldon, P.C. Morgan, K. Shimizu, Anodizing of aluminium in borax solution, Trans. IMF 77 (1999) 171-177.
47) S.J. Garcia-Vergara, P. Skeldon, G.E. Thompson, H. Habazaki, Formation of porous anodic alumina in alkaline borate electrolyte, Thin Solid Films 515 (2007) 5418-5423.
48) H. Ikeda, M. Iwai, D. Nakajima, T. Kikuchi, S. Natsui, N. Sakaguchi, R.O. Suzuki, Nanostructural characterization of ordered gold particle arrays fabricated via aluminum anodizing, sputter coating, and dewetting, Appl. Surf. Sci. 465 (2019) 747-753.
49) G.E. Thompson, Porous anodic alumina: fabrication, characterization and applications, Thin Solid Films 297 (1997) 192-201.
50) Y. Li, H. Shimada, M. Sakairi, K. Shigyo, H. Takahashi, M. Seo, Formation and breakdown of anodic oxide films on aluminum in boric acid/borate solutions, J. Electrochem. Soc. 144 (1997) 866-876.
51) H.O. Ali, P. Neufeld, Branching colony pore structure in anodic alumina films, Nat. Phys. Sci. 240 (1972) 14.
52) G.E. Thompson, R.C. Furneaux, G.C. Wood, Electron microscopy of ion beam thinned porous anodic films formed on aluminium, Corr. Sci. 18 (1978) 481-498.
53) J.E. Houser, K.R. Hebert, The role of viscous flow of oxide in the growth of self-ordered porous anodic alumina films, Nat. Mater. 8 (2009) 415-420.
54) K.R. Hebert, S.P. Albu, I. Paramasivam, P. Schmuki, Morphological instability leading to formation of porous anodic oxide films, Nat. Mater. 11 (2012) 162-166.
55) S.J. Garcia-Vergara, P. Skeldon, G.E. Thompson, H. Habazaki, A tracer investigation of chromic acid anodizing of aluminium, Surf. Interface Anal. 39 (2007) 860-864.
56) D. Elabar, A. Němcová, T. Hashimoto, P. Skeldon, G.E. Thompson, Effect of sulphate impurity in chromic acid anodizing of aluminium, Corr. Sci. 100 (2015) 377-385.
57) D. Nakajima, T. Kikuchi, S. Natsui, R.O. Suzuki, Advancing and receding contact angle investigations for highly sticky and slippery aluminum surfaces fabricated from nanostructured anodic oxide, RSC Adv. 8 (2018) 37315-37323.
58) K. Nakayama, E. Tsuji, Y. Aoki, H. Habazaki, Fabrication of superoleophobic hierarchical surfaces for low-surface-tension liquid, RSC Adv. 4 (2014) 30927-30933.

Figure Captions

Figure 1 Voltage-time curves during anodizing for Al in a 0.1 M $Na_2B_4O_7$ solution at a) 293 K, b) 313 K, and c) 333 K under various constant current densities.

Figure 2 SEM images of the surface of the specimens that are anodized in a 0.1 M $Na_2B_4O_7$ solution at a) 293 K and 2.5 Am^{-2} and b) 333 K and 75 Am^{-2}.

Figure 3 Voltage-time curves during anodizing in a) 0.05 M, b) 0.3 M, and c) 0.5 M $Na_2B_4O_7$ solutions at 333 K under various constant current densities.

Figure 4 SEM images of the surface (top) and the fracture cross-section (bottom) of the specimens that were anodized in a 0.3 M $Na_2B_4O_7$ solution at 333 K and a) 15 Am^{-2}, b) 30 Am^{-2}, and c) 50 Am^{-2}.

Figure 5 SEM images of the Al substrate after anodizing in a 0.3 M $Na_2B_4O_7$ solution 333 K and a) 25 Am^{-2} and b) 50 Am^{-2} and the subsequent selective dissolution of the porous alumina. c) The change in the cell size of the porous alumina, D_c, with the anodizing voltage, U_a.

Figure 6 High-magnification SEM images of the fracture porous alumina formed by anodizing in a) 0.3 M and b) 0.5 M $Na_2B_4O_7$ solutions at 333 K and 30 Am^{-2}.

Figure 7 a) A HAADF-STEM image of the horizontal cross-section of the porous alumina that was formed by anodizing in 0.5 M $Na_2B_4O_7$ solutions at 333 K and 30 Am^{-2}. b) A high-magnification HAADF-STEM image of a pore formed in the porous alumina. c)-e) BF-TEM images of the vertical cross-section of the porous alumina.

Figure 8 a) A HAADF-STEM image of the horizontal section of the porous alumina that formed by anodizing in 0.5 M $Na_2B_4O_7$ solutions at 333 K and 30 Am^{-2} and the corresponding elemental distribution maps of Al, O, and B. b) EDS spectrum of the anodized specimen shown in a). c) A HAADF-STEM image of the horizontal section of the porous alumina. d) EELS spectra of the anodic oxide shown in c).

Figure 9 Voltage-time curves during anodizing in a 0.5 M $Na_2B_4O_7$ solution at 353 K under various constant current densities.

Figure 10 SEM images of the surface (left), the fracture cross-section (center), and the Al dimple array (right) that were formed by anodizing in a 0.5 M $Na_2B_4O_7$ solution at 353 K and a) 150 Am^{-2} and b) 200 Am^{-2}.

Figure 11 Side views of the a) ultrapure water and b) rapeseed oil droplets that were formed on the SAM-modified Al specimen during the advancing contact angle (θ_{adv}) and the receding contact angle (θ_{rec}) measurements.

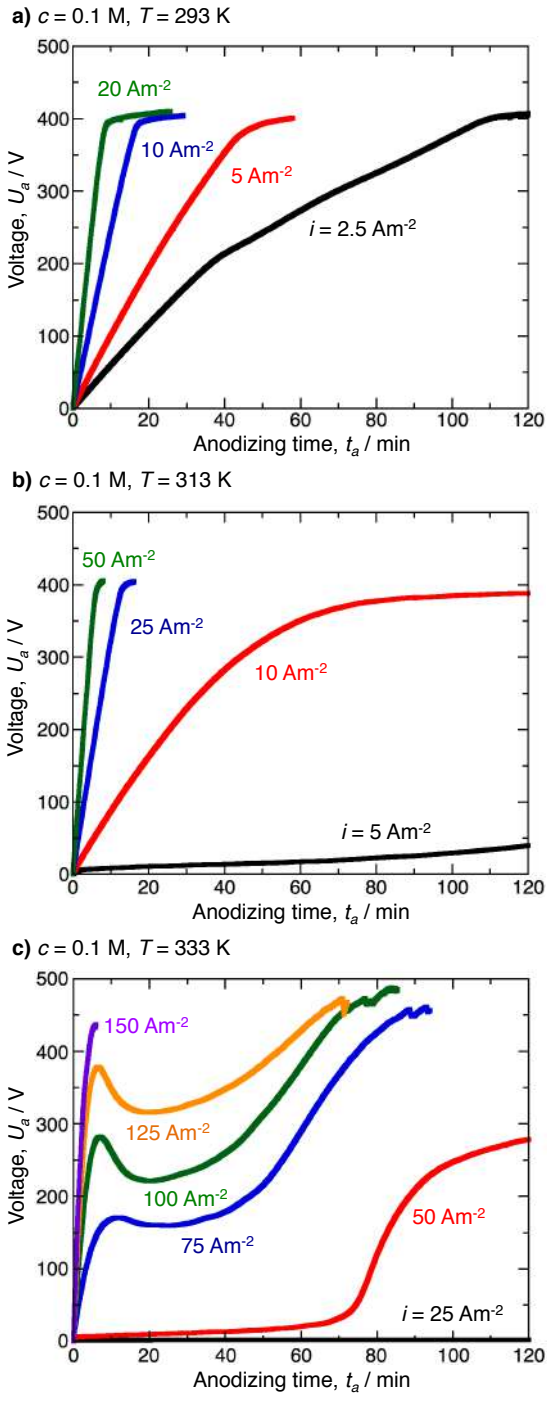
a) c = 0.1 M, T = 293 K
20 Am-2
10 Am-2
5 Am-2
i = 2.5 Am-2
Voltage, Ua / V
Anodizing time, ta / min
b) c = 0.1 M, T = 313 K
50 Am-2
25 Am-2
10 Am-2
i = 5 Am-2
Voltage, Ua / V
Anodizing time, ta / min
c) c = 0.1 M, T = 333 K
150 Am-2
125 Am-2
100 Am-2
75 Am-2
50 Am-2
i = 25 Am-2
Voltage, Ua / V
Anodizing time, ta / min

Figure 1.

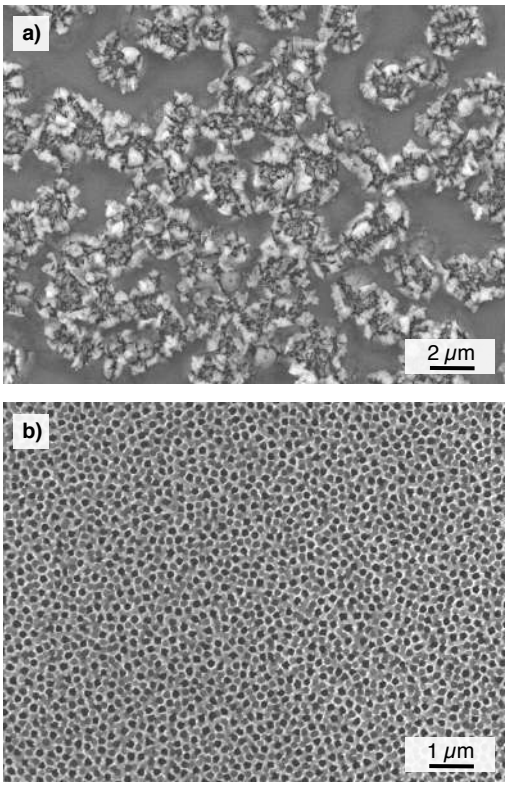

Figure 2.

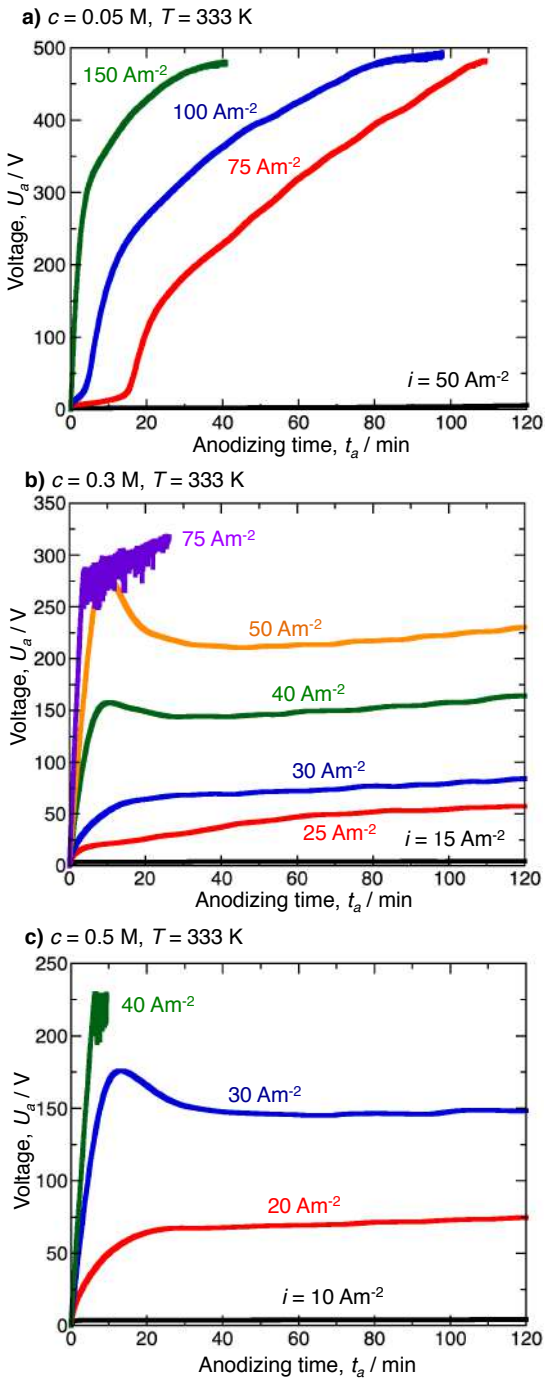
a) c = 0.05 M, T = 333 K
150 Am-2
100 Am-2
75 Am-2
i = 50 Am-2
Voltage, Ua / V
Anodizing time, ta / min
b) c = 0.3 M, T = 333 K
75 Am-2
50 Am-2
40 Am-2
30 Am-2
25 Am-2
i = 15 Am-2
Voltage, Ua / V
Anodizing time, ta / min
c) c = 0.5 M, T = 333 K
40 Am-2
30 Am-2
20 Am-2
i = 10 Am-2
Voltage, Ua / V
Anodizing time, ta / min

Figure 3.

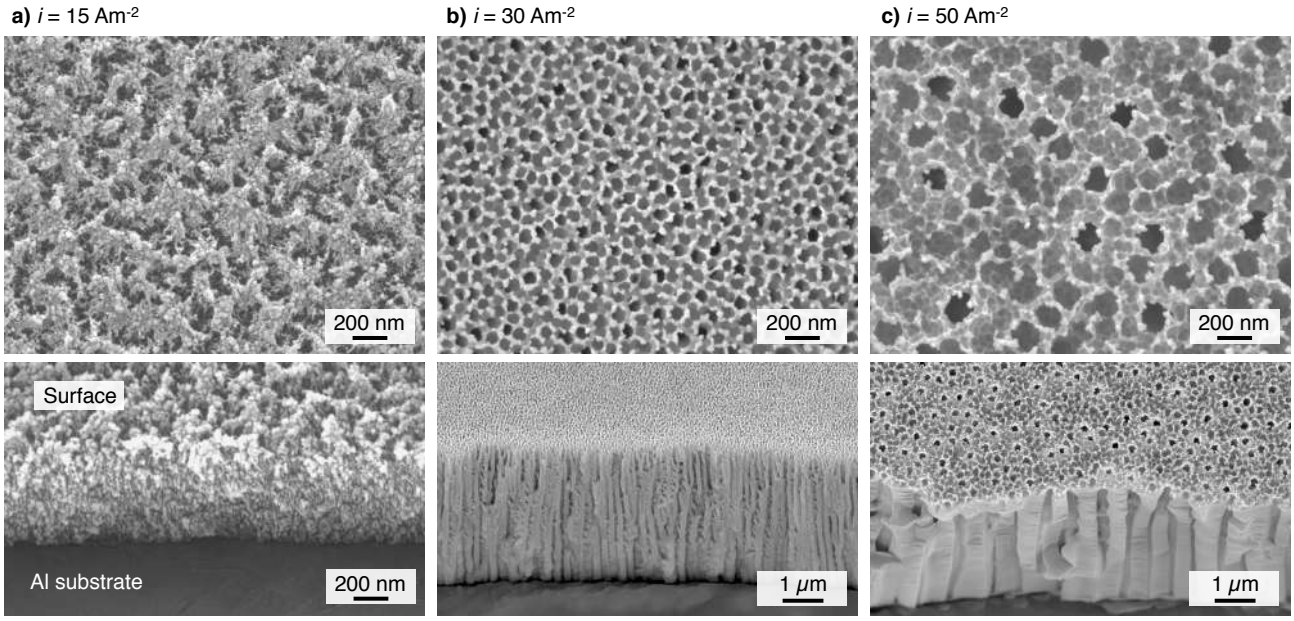
a) i = 15 Am-2
b) i = 30 Am-2
c) i = 50 Am-2
200 nm
200 nm
200 nm
Surface
Al substrate
200 nm
1 μm
1 μm

Figure 4.

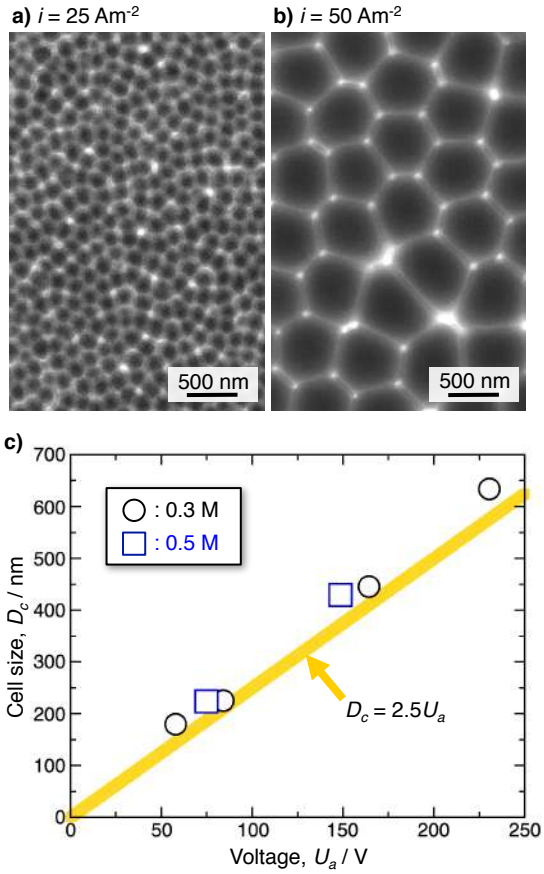
a) i = 25 Am^{-2}
b) i = 50 Am^{-2}
500 nm
500 nm
c)
: 0.3 M
: 0.5 M
$D_c = 2.5U_a$
Cell size, D_c / nm
Voltage, U_a / V
0
100
200
300
400
500
600
700
0
50
100
150
200
250

Figure 5.

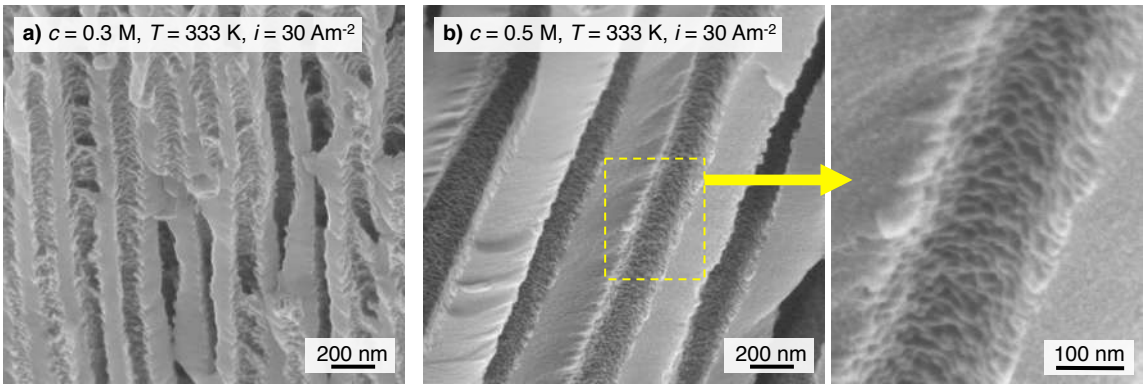

Figure 6.

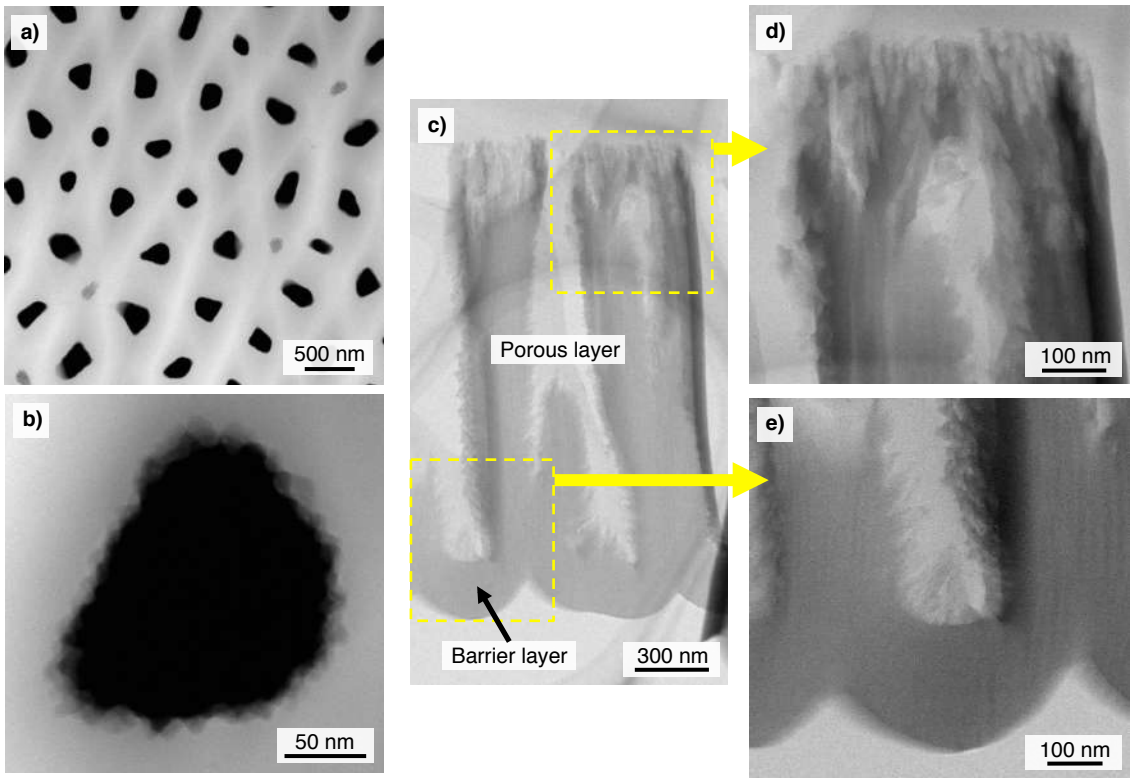
a)
500 nm
b)
50 nm
c)
Porous layer
Barrier layer
300 nm
d)
100 nm
e)
100 nm

Figure 7.

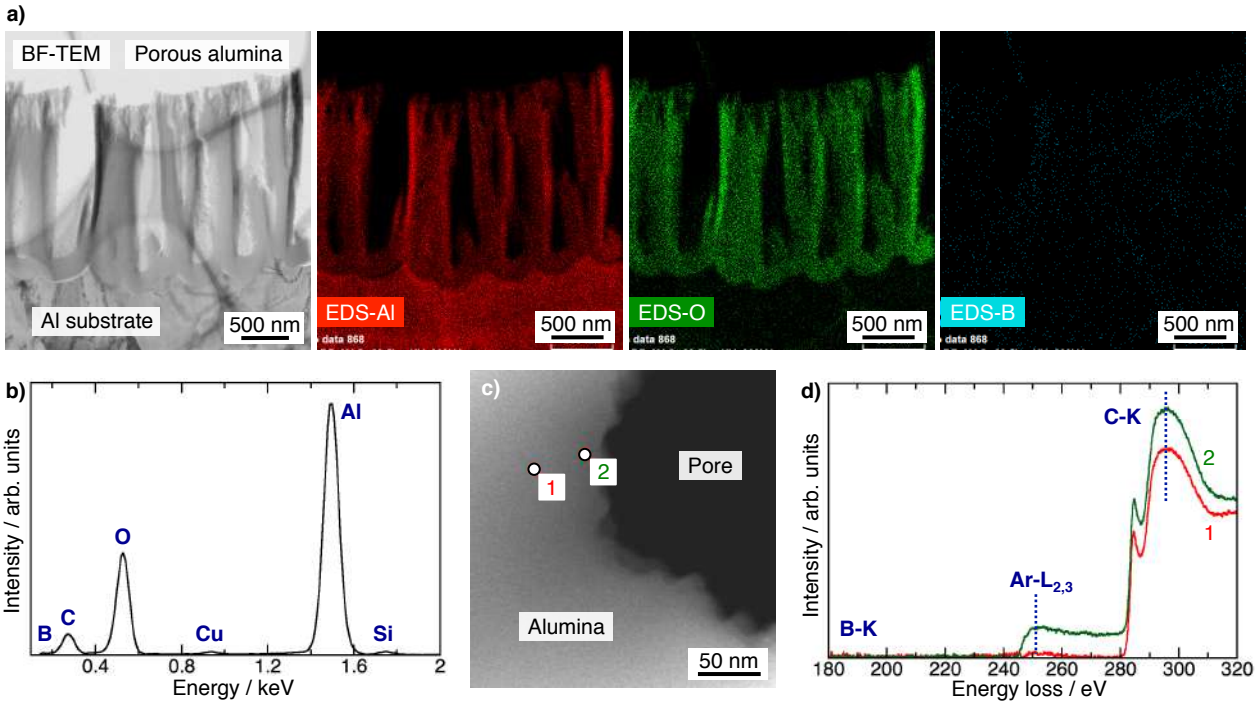
a)
BF-TEM
Porous alumina
Al substrate
500 nm
EDS-Al
500 nm
EDS-O
500 nm
EDS-B
500 nm
b)
Intensity / arb. units
B
C
O
Cu
Al
Si
0.4
0.8
1.2
1.6
2
Energy / keV
c)
1
2
Pore
Alumina
50 nm
d)
Intensity / arb. units
C-K
2
1
Ar-L2,3
B-K
180
200
220
240
260
280
300
320
Energy loss / eV

Figure 8.

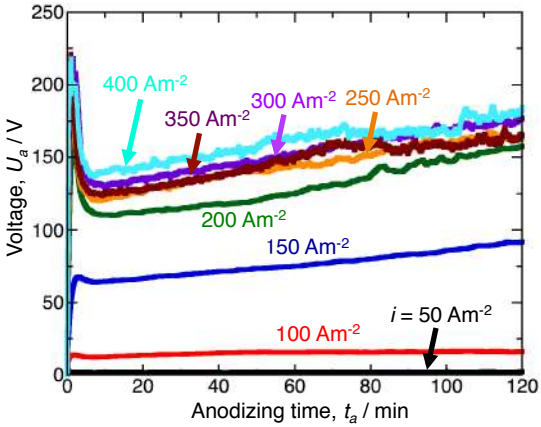
250
200
150
100
50
0
0
20
40
60
80
100
120
Voltage, U_a / V
Anodizing time, t_a / min
400 Am^{-2}
350 Am^{-2}
300 Am^{-2}
250 Am^{-2}
200 Am^{-2}
150 Am^{-2}
100 Am^{-2}
i = 50 Am^{-2}

Figure 9.

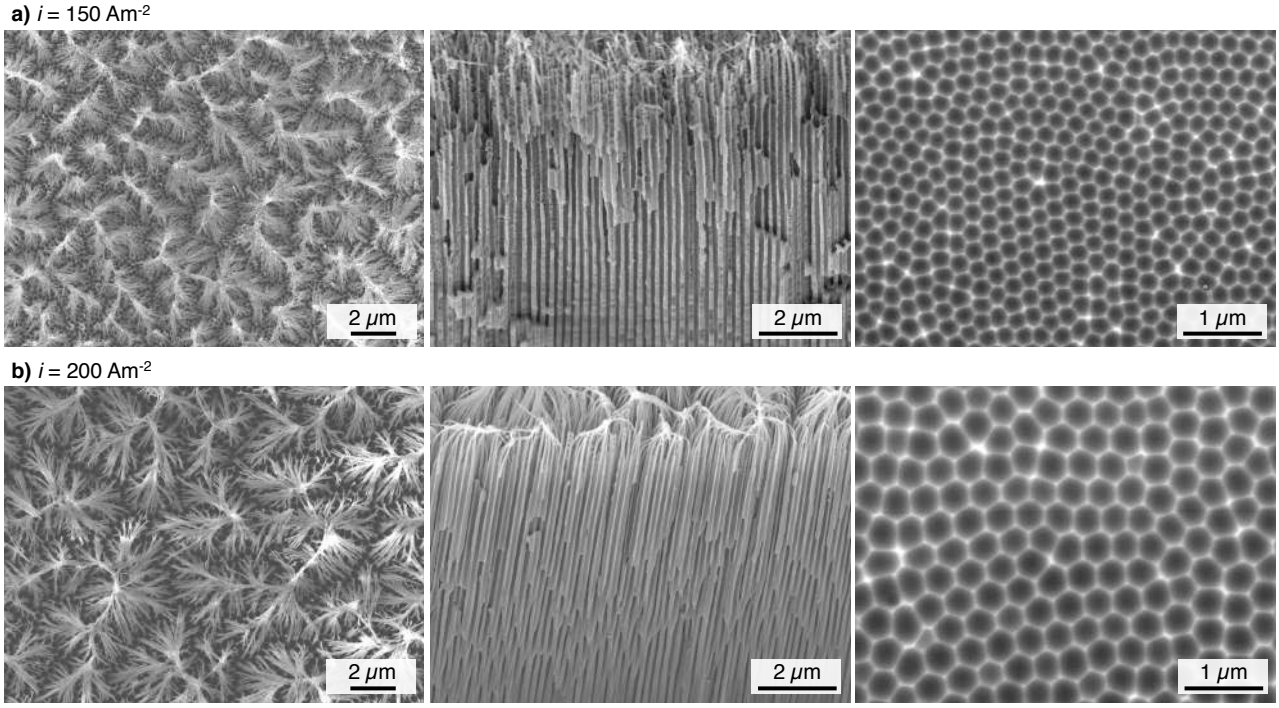

Figure 10.

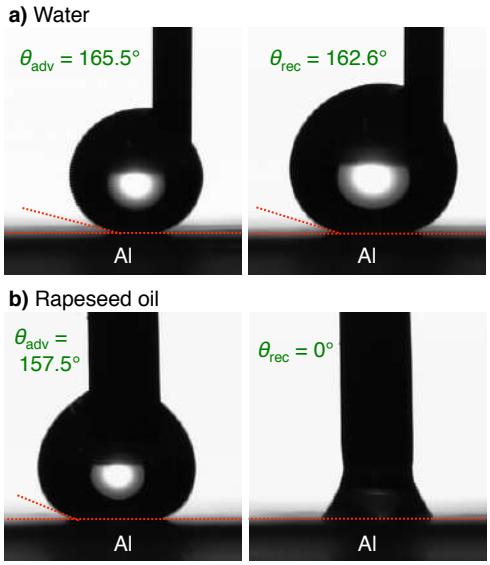
a) Water
θadv = 165.5°
θrec = 162.6°
Al
Al
b) Rapeseed oil
θadv = 157.5°
θrec = 0°
Al
Al

Figure 11.